



THE UNIVERSITY *of* EDINBURGH

## Edinburgh Research Explorer

### **Solar Activation of TiO<sub>2</sub> Intensified with Graphene for Degradation of Bisphenol-A in Water**

**Citation for published version:**

Monteagudo, JM, Duran, A, Chatzisyseon, E, San Martin, I & Naranjo, S 2018, 'Solar Activation of TiO<sub>2</sub> Intensified with Graphene for Degradation of Bisphenol-A in Water', *Solar Energy*, vol. 174, pp. 1035-1043. <https://doi.org/10.1016/j.solener.2018.09.084>

**Digital Object Identifier (DOI):**

[10.1016/j.solener.2018.09.084](https://doi.org/10.1016/j.solener.2018.09.084)

**Link:**

[Link to publication record in Edinburgh Research Explorer](#)

**Document Version:**

Peer reviewed version

**Published In:**

Solar Energy

**General rights**

Copyright for the publications made accessible via the Edinburgh Research Explorer is retained by the author(s) and / or other copyright owners and it is a condition of accessing these publications that users recognise and abide by the legal requirements associated with these rights.

**Take down policy**

The University of Edinburgh has made every reasonable effort to ensure that Edinburgh Research Explorer content complies with UK legislation. If you believe that the public display of this file breaches copyright please contact [openaccess@ed.ac.uk](mailto:openaccess@ed.ac.uk) providing details, and we will remove access to the work immediately and investigate your claim.



1  
2  
3  
4  
5  
6  
7  
8  
9 **Solar Activation of TiO<sub>2</sub> Intensified with Graphene for Degradation of**  
10 **Bisphenol-A in Water**  
11  
12

13 J.M. Monteagudo<sup>a\*</sup>, A. Durán<sup>a</sup>, E. Chatzisyneon<sup>b</sup>, I. San Martín<sup>a</sup>, S. Naranjo<sup>a</sup>  
14  
15  
16

17  
18 <sup>a</sup> *Department of Chemical Engineering, Grupo IMAES, Escuela Técnica Superior de Ingenieros*  
19 *Industriales, Instituto de Investigaciones Energéticas y Aplicaciones Industriales*  
20 *(INEI) University of Castilla-La Mancha, Avda. Camilo José Cela 3, 13071 Ciudad Real*  
21 *(Spain).*  
22

23 <sup>b</sup> *Institute for Infrastructure and Environment, School of Engineering, The University of*  
24 *Edinburgh, Edinburgh EH9 3JL, United Kingdom.*  
25  
26  
27  
28

29 \* To whom correspondence should be addressed

30  
31 Department of Chemical Engineering, Grupo IMAES  
32 Escuela Técnica Superior de Ingenieros Industriales,  
33 Instituto de Investigaciones Energéticas y Aplicaciones Industriales (INEI)  
34 University of Castilla-La Mancha,  
35 Avda. Camilo José Cela 3, 13071 Ciudad Real (Spain).  
36 Fax: 0034 926295361.  
37 Phone: 0034 926295300, ext: 3888  
38 Email: josemaria.monteagudo@uclm.es  
39

## ABSTRACT

Photocatalytic degradation of a Bisphenol-A (BPA) aqueous solution was achieved using titanium dioxide ( $\text{TiO}_2$ ) and graphene-based  $\text{TiO}_2$  photocatalysts activated by solar light. First, a comparative study of the adsorption kinetics of BPA, in the presence of both catalysts, as a function of pH was performed. Then, the effect of the initial BPA concentration and catalyst loading was assessed and the optimal conditions for BPA degradation by means of heterogeneous solar photocatalysis were determined. It was observed that  $\text{TiO}_2$  modified with 2 wt% graphene improved the photocatalytic efficiency in terms of BPA mineralization. The  $\text{TiO}_2$ /graphene photocatalytic composite achieved a 16% increase in the photocatalytic mineralization of the BPA solution under solar light compared to un-doped  $\text{TiO}_2$ . This enhancement of photocatalytic efficiency is a result of the increase of active sites for BPA adsorption, the more efficient harvesting of solar light, and the inhibition of electron-hole recombination. The dynamic behavior of hydroxyl radicals and dissolved oxygen in these systems was also discussed. Finally, the roles played by hydroxyl radical,  $\text{HO}^\bullet$ , superoxide radical anion,  $\text{O}_2^{\bullet-}$ , and singlet molecular oxygen,  $^1\text{O}_2$ , were studied in both  $\text{TiO}_2$  and  $\text{TiO}_2$ /graphene systems. It was found that  $\text{O}_2^{\bullet-}$  were the main oxidative species in both systems.

*Keywords: bisphenol-A;  $\text{TiO}_2$ /graphene; oxidative species; solar light.*

## 1. INTRODUCTION

Bisphenol-A (BPA) is a well-known endocrine disrupting chemical (EDC) that has been extensively detected in the environment. BPA can cause adverse health effects due to its interference with the human and animal hormones (Schafer et al., 1999; Gultekin et al., 2009; Rubin, 2011; Rogers et al., 2013). Due to its xenobiotic nature, this molecule cannot be completely degraded by the biological treatment processes used in wastewater treatment plants (WWTPs) and it is therefore discharged intact into the environment (Hu et al., 2007; Crain et al., 2007). Hence, an efficient treatment system for removing BPA or its oxidation reaction intermediates from the aquatic environment remains a pressing need for water industry and decision makers.

It is well-known that Advanced Oxidation Processes (AOPs) are effective methods for treating organic pollutants in water. The efficacy of AOPs is based on the generation of highly reactive free radicals, especially hydroxyl radicals ( $\text{HO}^\bullet$ ) or sulfate radicals ( $\text{SO}_4^{\bullet-}$ ), which are capable of transforming bio-recalcitrant molecules into biodegradable products. Among AOPs, heterogeneous photocatalytic degradation reactions using semiconductor metallic oxides, such as  $\text{TiO}_2$ , as photocatalysts to destruct persistent organic pollutants such as EDCs have been well studied (Esplugas et al., 2007; Durán et al., 2009; Xekoukoulotakis et al., 2011). Reactive oxygen species, mainly hydroxyl radical, superoxide radical anion,  $\text{O}_2^{\bullet-}$ , and singlet molecular oxygen,  $^1\text{O}_2$ , which can degrade a wide range of chemical contaminants in water, are generated during photocatalytic processes. However, the production of photons by means of artificial light sources requires a substantial amount of electrical energy (Pérez et al., 2002). Solar energy can be used, alternatively to UV lamps, as a more sustainable option in order to reduce the energy and costs of the water treatment process.  $\text{TiO}_2$ -assisted photocatalytic

degradation of several organic contaminants by solar light has been successfully used. This was found to be an economically viable process since solar energy is an abundant natural energy source and can be used instead of artificial light sources which are costly and hazardous (Konstantinou and Albanis, 2003; Robert et al., 2004).  $\text{TiO}_2$  has a wide band gap (anatase  $E_{\text{bg}} = 3.2 \text{ eV}$  or  $\lambda < 387 \text{ nm}$ ) and requires UV excitation (energy equal to or greater than the band-gap) to form electron-hole pairs. The conduction band electrons are able to reduce dissolved oxygen to generate superoxide radical,  $\text{O}_2^{\bullet-}$ , hydroperoxyl radicals,  $\text{HO}_2^{\bullet}$ , and through subsequent reduction reactions, hydrogen peroxide,  $\text{H}_2\text{O}_2$ , and hydroxyl radical,  $\text{HO}^{\bullet}$ . The valence band holes,  $\text{h}^+$ , are able to oxidize water to form  $\text{HO}^{\bullet}$ . The drawbacks of solar photocatalysis are that the UV radiation received by the earth is only around 5% of the entire solar energy spectrum and the photogenerated electron-hole pairs have fast recombination rates. In this sense, the efficiency of solar photocatalysis can be improved by doping  $\text{TiO}_2$  composites with materials, such as graphene (Kumordzi et al., 2016), in order to expand the catalyst band-gap to the visible light region of the solar spectrum ( $\lambda > 400 \text{ nm}$ ) and prevent electron-hole pair recombination (Fukahori et al., 2003; Bellobono et al., 2005; Ni et al., 2007; Fujishima et al., 2008). The use of graphene is of great scientific interest due to its excellent properties such as chemical inertness, stability in both acidic and basic mediums, its abundance and large surface area ( $2630 \text{ m}^2/\text{g}$ ) (Upadhyay et al., 2014).

BPA degradation has been previously investigated in many oxidative treatment processes, such as UV/ $\text{H}_2\text{O}_2$  and UV/persulfate (Yoon et al., 2012). A comparative study on the oxidative degradation of BPA by Fenton reagent, UV, UV/ $\text{H}_2\text{O}_2$  and Ultrasound has been also reported (Young et al., 2013). The removal of BPA by means of UV, UV/ $\text{H}_2\text{O}_2$ , UV/ $\text{K}_2\text{S}_2\text{O}_8$  and UV/ $\text{Na}_2\text{CO}_3$  processes was also studied (Sánchez-

Polo et al., 2013). F-TiO<sub>2</sub>-RGO nanocomposites were examined for BPA degradation under UV light illumination (Luoa et al., 2015). TiO<sub>2</sub>/graphene/Cu<sub>2</sub>O was applied in the photoelectrocatalytic oxidation of BPA under artificial visible light irradiation (Yanga et al., 2016). The catalytic ability of TiO<sub>2</sub>-reduced graphene oxide hybrid (TiO<sub>2</sub> – RGO) in photocatalysis using an artificial 365 nm light and ozonation combined system to degrade BPA was also investigated (Liao et al., 2016).

However, to the best of our knowledge, the application of graphene-TiO<sub>2</sub> composites irradiated by natural solar light for BPA degradation has not been studied yet. Therefore, further studies are required in this area to develop a more sustainable and cost efficient treatment technology. The aim of this work is to investigate BPA mineralization reactions by using solar photocatalytic oxidation in the presence of TiO<sub>2</sub> and TiO<sub>2</sub>/graphene composites. First, the influence of pH on BPA adsorption kinetics for both TiO<sub>2</sub> and TiO<sub>2</sub>/graphene composites was investigated. Then, the effects of various process parameters, such as initial concentrations of BPA and suspended photocatalysts as well as the type of the catalyst on mineralization reactions were evaluated. Afterwards, the dynamic behavior of HO• radicals and the profile of dissolved oxygen in both catalytic systems were determined. Finally, the roles played by different reactive oxidative species such as HO•, O<sub>2</sub>•<sup>-</sup> and <sup>1</sup>O<sub>2</sub>, in both TiO<sub>2</sub> and TiO<sub>2</sub>/graphene systems were evaluated using appropriate scavengers.

## **2. EXPERIMENTAL**

### *2.1. Materials*

BPA (CAS No: 80-05-7) (Fig. 1a), p-benzoquinone, sodium azide and ethanol (99.5%) were purchased from Sigma-Aldrich. Aeroxide® TiO<sub>2</sub> P25 was supplied by Evonik Industries and graphite powder (natural, microcrystal grade, product no. 14736) was purchased from Alfa Aesar. Tert-butyl alcohol was purchased from Panreac. All chemicals were used as received without further purification. The pH of the wastewater in each test was adjusted using H<sub>2</sub>SO<sub>4</sub> and NaOH solutions.

## *2.2. Photocatalyst preparation and characterization*

Graphite oxide, GO, was obtained from graphite powder through the modified Hummers method (Hummers and Offeman, 1958; Hassan et al., 2013). GO was dissolved in a water/ethanol (2:1) solution followed by 60 min ultrasound treatment. Then, a calculated amount (to obtain concentrations of 1, 2 and 3 wt% of graphene) of commercial TiO<sub>2</sub> nanoparticles (P25) was added to the GO solution, which was continuously stirred for 3 h. The mixture was transferred to a Teflon-lined autoclave, and the hydrothermal process was performed at 120 °C for 15 h. During this process, GO could be reduced to graphene and the deposition of TiO<sub>2</sub> was achieved. Then, the obtained composites were centrifuged, rinsed with deionized water, and dried at 60°C. The prepared samples are denoted as TiO<sub>2</sub>/graphene.

Structural analyses of TiO<sub>2</sub> and TiO<sub>2</sub>/graphene samples were determined by X-ray Diffraction (XRD) using a PHILIPS X'Pert MPD PW 3040 analyzer with a Cu KAlpha1 radiation. Ultraviolet-visible (UV-Vis) spectra were collected in a Cary 100 diffuse reflectance UV-Vis spectrophotometer. Transmission electron microscopy

(TEM) images were obtained using a JEOL JEM-2100Plus microscope. The specific surface area, pore size and pore volume of the samples was measured with Brunauer-Emmett-Teller (BET) method using the Micro-meritics Gemini VII 2390 by using N<sub>2</sub> adsorption at 77 K.

### *2.3. Experimental set-up*

Fig. 1b illustrates the scheme of the experimental set-up. A CPC solar reactor with a surface of 0.25 m<sup>2</sup>, manufactured by Ecosystem, S.A., consisted of 2 borosilicate tubes and an irradiated volume of 2 L. The reactor was mounted on a fixed south-facing platform tilted 39° in Ciudad Real (Spain). It included a continuously stirred tank (volume= 1.5 L) and a centrifugal recirculation pump (flow rate: 30 L min<sup>-1</sup>).

### *2.4. Adsorption studies*

To analyze BPA adsorption on TiO<sub>2</sub> or TiO<sub>2</sub>/graphene composites, different experiments were conducted in the dark using the experimental reactor indicated above. 3.5 L of aqueous solution containing 10 mg L<sup>-1</sup> BPA solution were prepared by weighing and dissolving, by ultrasound mixing for 3 hours, the appropriate amount of BPA in deionized water. Then, the appropriate amount of catalyst (TiO<sub>2</sub> alone or TiO<sub>2</sub>/graphene) was added to the solution to reach a concentration of 125 mg L<sup>-1</sup> TiO<sub>2</sub>. Solution pH can affect both the adsorbent electrical surface charge and the dissociation of the adsorbate. The effect of pH on adsorption of BPA by TiO<sub>2</sub> or by TiO<sub>2</sub>/graphene was studied fixing the initial pH value of the solutions at 7.5 and 2.5. These pH values



were chosen taking into account the point of the zero charge (PZC) of  $\text{TiO}_2$  (between  $\text{pH} = 5.6$  and  $6.4$  (Daneshvar et al., 2004). It is well-known that the surface charge of  $\text{TiO}_2$  depends on  $\text{pH}$ . At more acidic  $\text{pH}$  values, the  $\text{TiO}_2$  surface is positively charged and above  $\text{TiO}_2$  PZC, the surface is negatively charged.

Samples were agitated at room temperature for a period of 2 h before being filtered through  $0.45\ \mu\text{m}$  syringe filters to separate catalyst particles and to analyze the residual concentrations of BPA.

#### *2.5. Solar photocatalytic process*

In a typical solar  $\text{TiO}_2$  or  $\text{TiO}_2/\text{graphene}$  photocatalytic run, BPA was dissolved in deionized water as indicated above. This BPA solution was then transferred into a reservoir and the appropriate pre-weighted amount of  $\text{TiO}_2$  or  $\text{TiO}_2/\text{graphene}$  catalyst was added in it. The BPA solution was stirred in the dark for 30 minutes to attain adsorption equilibrium between BPA and catalyst particles. The reactant mixture was then pumped through the CPC and solar photocatalytic oxidation started. During the experiments, samples were periodically withdrawn from the reactor and filtered through  $0.45\ \mu\text{m}$  syringe filters to separate catalyst particles from the liquid. Chemical analyses for BPA,  $\text{HO}^\bullet$ , Total Organic Carbon (TOC) and dissolved oxygen content were performed.

To quantify the oxidation levels by  $\text{HO}^\bullet$ ,  $\text{O}_2^{\bullet-}$  and  $^1\text{O}_2$ , 1 M tert-butyl alcohol, 2 mM 1,4-benzoquinone and 2 mM sodium azide were used as scavenging agents, respectively.

All experiments were performed in triplicate, and the medium values were used. Before analysis, all filtered samples were immediately treated with excess  $\text{Na}_2\text{SO}_3$  to prevent further oxidation (this procedure was performed to avoid overestimating degradation). All the experiments were conducted at room temperature and at natural pH of BPA solution ( $\cong 7.5$ ).

## 2.6. Analysis

BPA concentration was determined using high-performance liquid chromatography with UV detection (Agilent Technologies 1100 HPLC-UV) in the isocratic mode immediately after sampling. An Eclipse XDB-C18 column (5 mm,  $4.6 \times 250$  mm) was used, and a 75:25 (v/v) methanol/(water with 1% acetic acid) mixture with an acidic pH was used as the mobile phase (detection wavelength,  $\lambda = 225$  nm; flow rate of  $0.6 \text{ ml min}^{-1}$ ). The mineralization grade of the treated wastewater was determined using a TOC analyzer (TOC-5050 Shimadzu, standard deviation  $< 0.2 \text{ mg L}^{-1}$ ). Quantification of hydroxyl radicals was carried out by fluorescence measurement using disodium salt of terephthalic acid (NaTA) (Saran and Summer, 1999). Dissolved oxygen concentration was measured using a Jenway 9200  $\text{DO}_2$  meter.

### 3. RESULTS AND DISCUSSION

#### 3.1. Characterization Results

##### *Surface area and porosity measurement*

The specific surface area, pore volume, and the pore size of the samples are summarized in Table 1. The BET surface area of the TiO<sub>2</sub> increased (10 %) with graphene incorporation, indicating that the physical adsorptivity of the nanocomposite was improved. This is presumably due to the high theoretical specific surface area (2600 m<sup>2</sup>/g) of reduced graphene oxide (Akhavan and Ghaderi, 2009). The pore size distribution was also estimated using the Barrett-Joyner-Halenda (BJH) method (Lellala et al., 2016) from the desorption branch of the isotherm. It can be seen that compared to the pure TiO<sub>2</sub>, the pore volume of TiO<sub>2</sub>/graphene was increased, which is vital to improve the adsorption capacity of the nanocomposite and to increase the efficiency of separation of electron-hole pairs (Saha et al., 2012). In addition, the values showed average pore diameter characteristic of mesoporous materials, which is important for photocatalytic applications.

##### *UV-Vis diffusive reflectance spectroscopy*

The TiO<sub>2</sub> absorption capacity can be studied by UV-Vis diffusive reflectance spectroscopy. Fig. 2 shows that both pure TiO<sub>2</sub> and TiO<sub>2</sub>/graphene have high absorption capacities in the UV region. However, only TiO<sub>2</sub>/graphene composite exhibited a broad adsorption spectra in the visible region. That shows the possibility of visible light photocatalyst by TiO<sub>2</sub>/graphene composite.

## 257 *X-Ray diffraction (XRD)*

258 X-Ray diffraction (XRD) was used to examine the crystalline structure of  $\text{TiO}_2$  and  
259  $\text{TiO}_2/\text{graphene}$  2 wt%. Figs. 3a and 3b show XRD patterns obtained for  $\text{TiO}_2$  and  
260  $\text{TiO}_2/\text{graphene}$ , respectively. As it is shown,  $\text{TiO}_2/\text{graphene}$  exhibited a similar XRD  
261 pattern to pure  $\text{TiO}_2$ . Anatase and rutile crystalline phases were observed in both  
262 composites. Peaks associated only with  $\text{TiO}_2$  were observed and no peak was assigned  
263 to GO. This indicates that GO was reduced to graphene during the hydrothermal  
264 treatment. Graphene did not affect the crystalline structure of  $\text{TiO}_2$ . The XRD patterns  
265 of the samples revealed the crystalline structure of the anatase  $\text{TiO}_2$  phase due to the  
266 presence of a distinct diffraction peak at  $2\theta$  of  $25.2^\circ$  that correspond to the  $\{011\}$  crystal  
267 plane. This peak and their corresponding reflections agree with ICSD collection code n°  
268 96946 for anatase. The peak diffraction of the rutile  $\text{TiO}_2$  phase was observed at  $2\theta$  of  
269  $27.4^\circ$  corresponding to the  $\{110\}$  crystal plane (ICSD collection code n° 76172). The  
270 proportion anatase: rutile and the maximum intensities of the peaks of anatase and rutile  
271 phases in the diffractograms were almost the same in both samples (anatase: rutile:  
272 87:13 for  $\text{TiO}_2$  and 86:14 for  $\text{TiO}_2/\text{graphene}$ ; maximum intensities: 509 and 76 counts,  
273 respectively, for  $\text{TiO}_2$  and 524 and 87 counts, respectively, for  $\text{TiO}_2/\text{graphene}$ ). It is well  
274 known that the intensity of the diffracted peak from a given crystalline structure of the  
275 element (i.e., anatase or rutile phase) is proportional to the amount of the structural  
276 element present in the crystal sample. The  $\text{TiO}_2$  modified with graphene did not suffer  
277 modifications in its crystalline structure. It is well-known that anatase form has a  
278 photocatalytic activity greater than rutile (Wang and Yu, 2013) which indicates that  
279 anatase can generate more oxidative species than rutile and besides the recombination  
280 rate of holes and electrons is lower in the anatase phase than in the rutile phase.

281

Figs. 3c-f present the TEM images of TiO<sub>2</sub>/graphene-2 wt% nanocomposite. It can be seen clearly the spherical TiO<sub>2</sub> nanoparticles and the graphene oxide sheets, which is covered with TiO<sub>2</sub> nanoparticles. Intraparticle aggregation formed a mesoporous structure, which was previously confirmed by nitrogen adsorption–desorption analysis. The average diameter of TiO<sub>2</sub> nanoparticles was about 10–30 nm, which is in agreement with the mean crystal size value of 19 nm estimated by the Scherrer equation (Patterson, 1939) based on (200) peak from the X-ray diffractogram.

### 3.2 Bisphenol-A adsorption kinetics

TiO<sub>2</sub> and TiO<sub>2</sub>/graphene particles consist of different adsorption sites which will define the adsorption ability of each catalyst. Two models were tested to analyze BPA adsorption: a) Lagergren model, a pseudo-first-order adsorption rate equation (Lagergren, 1898) and b) Ho and McKay model, pseudo-second-order adsorption rate equation (Ho and McKay, 1999).

The Lagergren equation can be represented by the following equation:

$$\frac{dQ_t}{dt} = k_1(Q_e - Q_t) \quad (1)$$

where  $Q_e$  and  $Q_t$  are the values of BPA mass adsorbed per unit mass of adsorbent at equilibrium and time  $t$  (mg g<sup>-1</sup>), respectively, and  $k_1$  is the pseudo-first-order rate constant (min<sup>-1</sup>). The integration of Eq (1) gives the following equation:

$$\log(Q_e - Q_t) = \log(Q_e) - \frac{k_1}{2.303} t \quad (2)$$

306

307 Plot of  $\log (Q_e - Q_t)$  versus  $t$  would yield a straight line if the adsorption follows a  
 308 pseudo-first order kinetic behaviour. This model is based on the assumption that the  
 309 adsorption rate depends on the number of adsorption sites on the adsorbent surface  
 310 (Lagergren, 1898). Figs. 4a and 4b show the kinetics of adsorption of BPA on the  $\text{TiO}_2$   
 311 and  $\text{TiO}_2/\text{graphene}$  surface, respectively, at both pH values, 2.5 and 7.5. We can see that  
 312 the pseudo-first-order kinetics for both systems,  $\text{TiO}_2$  and  $\text{TiO}_2/\text{graphene}$ , was found to  
 313 be suitable only for an initial interaction time (up to 60 min) and not for the 120 min of  
 314 total contact time.

315 The pseudo-second order kinetic model (Ho and McKay model), given by Eq (3) is  
 316 based on the assumption that the adsorption rate is determined by the square of the  
 317 number of vacant adsorption sites on the adsorbent surface (Ho and McKay, 1999).

318

$$\frac{dQ_t}{dt} = k_2(Q_e - Q_t)^2 \quad (3)$$

320

321 where  $Q_e$  and  $Q_t$  are the values of BPA mass adsorbed per unit mass of adsorbent at  
 322 equilibrium and time  $t$  ( $\text{mg g}^{-1}$ ), respectively, and  $k_2$  is the pseudo-second-order rate  
 323 constant ( $\text{g min}^{-1} \text{mg}^{-1}$ ). The integration of Eq (3) gives the following expression:

324

$$\frac{t}{Q_t} = \frac{1}{k_2(Q_e)^2} + \frac{1}{Q_e} t \quad (4)$$

326

327 Figs. 4c and 4d show the plot of  $t/Q_t$  versus  $t$  for the adsorption of BPA by  $\text{TiO}_2$  and  
328  $\text{TiO}_2/\text{graphene}$  catalysts, respectively, for the two studied pH values, 2.5 and 7.5. As it  
329 can be seen, the data fit well to a pseudo-second-order rate kinetics at both pH values  
330 for the whole contact time. As shown in Table 2, it can be concluded that: (i) the  $k_2$   
331 values are higher for BPA adsorption on  $\text{TiO}_2/\text{graphene}$  than in pure  $\text{TiO}_2$ ; (ii) in both  
332 systems,  $k_2$  values depend on the medium pH being higher at pH 7.5 since it takes a  
333 shorter time to reach equilibrium (values of  $k_2(\text{BPA-TiO}_2) = 0.0007$  and  $0.0037 \text{ g min}^{-1}$   
334  $\text{mg}^{-1}$  at pH 2.5 and 7.5, respectively, and  $k_2(\text{BPA-TiO}_2/\text{graphene}) = 0.0029$  and  $0.0043 \text{ g}$   
335  $\text{min}^{-1} \text{ mg}^{-1}$  at pH 2.5 and 7.5, respectively. This may be explained by the abatement of  
336 hydrogen ions after the increase of pH, which reduces the chance of competition  
337 between hydrogen ions and the BPA molecules. Due to the natural negative charge of  
338  $\text{TiO}_2$  at  $\text{pH} > \text{PZC}$  and the natural negative charge of GO over this whole pH range, it  
339 would be possible for hydrogen ions to be adsorbed by  $\text{TiO}_2$  and  $\text{TiO}_2/\text{graphene}$  through  
340 electrostatic interactions. On the other hand, at  $\text{pH} < 4.5$ , catalyst particles  
341 agglomeration could reduce the BPA adsorption as well as photon absorption  
342 (Muruganandham and Swaminathan, 2004); (iii) the adsorption capacity,  $Q_e$ , of BPA by  
343  $\text{TiO}_2/\text{graphene}$  catalyst is higher than that by pure  $\text{TiO}_2$  being approximately 31 and 18  
344  $\text{mg g}^{-1}$ , respectively.

345

346 When adsorption data follow a pseudo-second-order kinetics, the rate limiting step may  
347 be chemical adsorption. The excellent adsorption ability may be attributed to  $\pi$ - $\pi$   
348 stacking interaction and hydrogen bond between BPA and graphene in agreement with  
349 other authors (Shen et al., 2014; Jin et al., 2015). Taking into account these adsorption

results and the natural pH of BPA solution ( $\cong 7.5$ ), this value of pH was chosen as optimal pH for all the photocatalytic experiments.

### *3.3 Degradation of BPA by solar TiO<sub>2</sub> process*

The degradation reaction of BPA solutions using a solar/TiO<sub>2</sub> photocatalytic system was investigated to find out the optimal values for the initial concentrations of BPA and TiO<sub>2</sub> being 2.5 mg L<sup>-1</sup> and 250 mg L<sup>-1</sup> the selected values, respectively (Figs. S1-S4, Supplementary Material).

### *3.4 Degradation of Bisphenol-A by solar graphene-based TiO<sub>2</sub> process*

To evaluate the performance of the catalytic activity of the TiO<sub>2</sub>/graphene catalyst, the degradation of 2.5 mg L<sup>-1</sup> BPA aqueous solution using 250 mg L<sup>-1</sup> TiO<sub>2</sub>/graphene catalyst (1, 2 and 3 wt% graphene concentrations with respect to TiO<sub>2</sub>) under natural solar light was tested. The initial pH was 7.5 in all experiments. The solar power was around 25-30 W/m<sup>2</sup>, and the average temperature was around 26°C in all experiments. Fig. 5a shows an enhancement in the mineralization efficacy of the BPA solution with the TiO<sub>2</sub>/graphene catalyst compared to TiO<sub>2</sub> alone. The percentage of TOC removal increased when TiO<sub>2</sub> was modified with amounts of graphene up to 2 wt%. Fig. 5b exhibits that the incorporation of graphene enhances their photoactivity for BPA mineralization. As can be observed, as the weight percentage of graphene increased from 0 to 2% at a fixed catalyst concentration of TiO<sub>2</sub> (250 mg L<sup>-1</sup>) the pseudo-first-order kinetic rate constant increased from 0.0128 to 0.0149 min<sup>-1</sup>, respectively, which



indicates about 16% improvement over that of pure TiO<sub>2</sub> catalyst. This improvement on the performance of TiO<sub>2</sub>/graphene could be due to the following: (a) the increase of catalytic surface active sites for the adsorption of BPA, as was discussed in the previous section, resulting in a more efficient photocatalytic process, (b) a good assembly and interfacial coupling between TiO<sub>2</sub> and graphene sheets, as observed by TEM images (Figs. 3c-f), could promote charge migration between both phases and increase the catalyst efficiency, (c) graphene when combined with TiO<sub>2</sub> reduced charge recombination, facilitating the electron-hole separation and the availability of photo-generated e<sup>-</sup> for the photocatalytic reaction, and (d) the introduction of graphene allowed a more efficient utilization of the solar spectrum (Malekshoar et al., 2014). It may note that when 3 wt% of graphene was used, the mineralization efficiency was lower possibly because the photoactivity of the catalyst decreased due to an increase in catalyst agglomerate size and a decrease in light penetration.

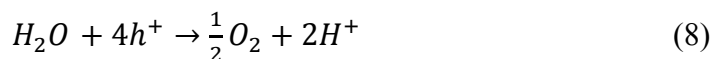
### *3.5 HO• and dissolved O<sub>2</sub> behavior in solar/TiO<sub>2</sub> and solar/TiO<sub>2</sub>/graphene*

Figs. 6a and 6b show the behavior of hydroxyl radical and dissolved oxygen, respectively, along BPA degradation reactions by means of the solar/TiO<sub>2</sub> process and for different initial concentrations of the organic pollutant. The initial concentration of BPA varied between 2.5 and 10 mg L<sup>-1</sup> in the presence of 125 mg L<sup>-1</sup> TiO<sub>2</sub>. The solar power in these experiments was around 25-30 W/m<sup>2</sup>, and the average temperature was 26°C. The reaction time was 120 min in all experiments. As it can be seen, when an initial concentration of BPA below 5 mg L<sup>-1</sup> was used, the concentration of HO• rapidly increased reaching a maximum value at around 6-10 min and then it remained constant.

Above 5 mg L<sup>-1</sup> BPA, the increase of the hydroxyl concentration was much lower reaching values of approximately 2000 and 500 nmol L<sup>-1</sup> for 7.5 and 10 mg L<sup>-1</sup> BPA, respectively. The greater concentration of HO• (≅ 13500 nmol L<sup>-1</sup>) was obtained using the smaller concentration of BPA, 2.5 mg L<sup>-1</sup>, being higher both the BPA and TOC removal in this case due to the higher TiO<sub>2</sub> photocatalytic efficiency, as indicated above.

Fig. 6b shows measurements of dissolved oxygen concentration during the solar/TiO<sub>2</sub> process at different initial BPA concentrations. It can be observed that the behaviour of dissolved oxygen was similar in all experiments although its concentration was lower when the initial BPA concentration was increased. In the first reaction stage, dissolved oxygen was decreased by reacting with the photo-excited electrons in the conduction band (Eq. (5)), thus generating superoxide radical anion, O<sub>2</sub><sup>•-</sup>. During this time period, solution TOC decreased (see Fig. S2, Supplementary Material). In a second reaction phase, after 90 min, when TOC remained constant, possibly due to the formation of recalcitrant intermediates, hard to be degraded, the concentration of dissolved O<sub>2</sub> was slightly increased according to reactions (6)-(8).





Figs. 6c and 6d show the behavior of hydroxyl radical and dissolved oxygen during BPA treatment by the solar/TiO<sub>2</sub> process in the presence of different initial TiO<sub>2</sub> concentrations of TiO<sub>2</sub> (between 100 and 500 mg L<sup>-1</sup>). For the sake of comparison, results during BPA treatment by means of the solar/TiO<sub>2</sub>/graphene (250 mg L<sup>-1</sup> TiO<sub>2</sub>/2wt% of graphene) system are also shown in these figures. The initial concentration of BPA was fixed at 5 mg L<sup>-1</sup>. The solar power in these experiments was around 25-30 W/m<sup>2</sup>, and the average temperature was 26°C. The reaction time was 120 min in all experiments. It can be seen that, in the solar/TiO<sub>2</sub> process, the increase of TiO<sub>2</sub> loading from 100 to 250 mg L<sup>-1</sup> led to the increase in HO• generation due to the increase of active sites on the catalyst surface and consequently to the increase in the photocatalytic yield and percentage of BPA and TOC removal, as indicated above. It can be also seen the reduction in the production of HO• when the initial concentration of TiO<sub>2</sub> was 500 mg L<sup>-1</sup>, justifying the degradation results indicated above. Also, Fig. 6c shows the behavior of HO• when TiO<sub>2</sub>/graphene (250 mg L<sup>-1</sup> TiO<sub>2</sub> with 2 wt% of graphene) irradiated by solar light was used. In this case, the concentration of HO• showed a similar tendency and it was slightly higher than under the same conditions in the presence of pure TiO<sub>2</sub> catalyst. This could be attributed to the consumption of HO• by reaction with superoxide radical, O<sub>2</sub>•<sup>-</sup>, to form singlet molecular oxygen, in the solar/TiO<sub>2</sub> process as given in Eq. (9):



445

446 With respect to the dissolved oxygen, Fig. 6d showed a similar behavior of  $O_2$  in the  
447 BPA solution although its values were slightly higher when the initial  $TiO_2$  loading  
448 increased in the solar/ $TiO_2$  treatment process. This could be attributed to higher rates of  
449 recombination of electrons and holes, which decreased the availability of  
450 photogenerated electrons,  $e^-_{CB}$ , to react with oxygen. However, as can be also seen in  
451 Fig. 6d, when  $TiO_2$  was modified with graphene (250 mg  $L^{-1}$   $TiO_2$  and 2 wt% of  
452 graphene) a more pronounced decrease of dissolved oxygen was observed, possibly due  
453 to a higher amount of  $e^-_{CB}$  on the catalyst surface which consumed more  $O_2$  forming  
454 superoxide radical and therefore inhibiting the hole/electron recombination. Thus, the  
455 photocatalytic efficacy was higher in the solar  $TiO_2$ /graphene treatment process as  
456 indicated above.

457

### 458 *3.5 Role of different oxidative intermediate species*

459

460 The contributions of various oxidative intermediate species to the degradation of BPA  
461 using both solar/ $TiO_2$  and solar/ $TiO_2$ /graphene processes were also examined. To  
462 quantify the oxidation levels by free radical reactions, the scavenging of intermediate  
463 active species was accomplished with 1 M concentration of tert-butyl alcohol ( $HO^\bullet$  and  
464  $HO_2^\bullet$  quencher), 2 mM 1,4-benzoquinone ( $O_2^{\bullet-}$  quencher) and 2mM sodium azide ( $^1O_2$   
465 quencher) (Li et al., 2009; Monteagudo et al., 2011). Several additional experiments  
466 under solar/ $TiO_2$  and solar/ $TiO_2$ /graphene process were carried out at the optimal  
467 conditions in the presence or absence of these scavengers. In these reactions, various  
468 oxidative intermediate species could be generated, such as the hydroxyl radical ( $HO^\bullet$ ),

hydroperoxyl ( $\text{HO}_2^\bullet$ ), singlet oxygen ( $^1\text{O}_2$ ), and the superoxide radical anion ( $\text{O}_2^{\bullet-}$ ). The roles of these species are shown in Figs. 7a and 7b. As shown, the presence of some scavenging agents inhibited the degradation reaction (the %BPA removal decreased as compared with the scavenger-free reaction). This indicates the participation of these species in the reaction. Superoxide radical anion,  $\text{O}_2^{\bullet-}$ , was found to be the primary species contributing to the degradation of BPA in both solar/ $\text{TiO}_2$  and solar/ $\text{TiO}_2$ /graphene systems since p-benzoquinone was the most significant scavenging agent. In the case of  $\text{TiO}_2$ /graphene treatment system, this may be due to the formation of a heterojunction interface in the  $\text{TiO}_2$ /graphene composites, where there is a space-charge separation region, graphene nanosheets can accept photogenerated electrons from the  $\text{TiO}_2$  conduction band. This reduced the electron-hole pair recombination, and subsequently the oxygen molecules adsorbed on the catalyst surface act as electron scavengers and combine with  $e^-_{CB}$  to form  $\text{O}_2^{\bullet-}$ , according to reaction (5) indicated above.  $\text{O}_2^{\bullet-}$  is in an acid-base equilibrium (Eq. (6)) but these species predominated over  $\text{HO}_2^\bullet$  since the medium pH was around 7 ( $\text{pK}_a(\text{HO}_2^\bullet) = 4.8 \pm 0.1$ ) (Bielski et al., 1985).

From Fig. 7, it can be also concluded that singlet molecular oxygen,  $^1\text{O}_2$ , played a role in the degradation of BPA, but it was more significant in the pure  $\text{TiO}_2$  rather than in the  $\text{TiO}_2$ /graphene treatment system.  $^1\text{O}_2$  is formed by  $\text{O}_2^{\bullet-}$  oxidation by holes,  $h^+$ , according to Eq. (10):



In the case of solar/ $\text{TiO}_2$  treatment reaction, the role played by hydroxyl radical,  $\text{HO}^\bullet$ , was less significant than that played by singlet oxygen. This could be attributed to the participation of  $\text{HO}^\bullet$  radicals instead of  $h^+$  in Eq. (10) as given in Eq (9) (Daimon et al.,

2008), thus decreasing the availability of hydroxyl radicals for the degradation reaction. However, the role of  $\text{HO}^\bullet$  was more significant than that played by  $^1\text{O}_2$  in the degradation of BPA under the solar  $\text{TiO}_2$ /graphene process possibly due to the higher availability of  $\text{h}^+$  as indicated above. In this case, the contribution of  $\text{HO}^\bullet$  to the  $^1\text{O}_2$  formation was less significant in comparison with the oxidation by  $\text{h}^+$ .

#### 4. Conclusions

The solar photocatalytic degradation and mineralization of a BPA aqueous solution in the presence of  $\text{TiO}_2$ /graphene composites was compared to that of pure  $\text{TiO}_2$  photocatalyst. The  $\text{TiO}_2$ /graphene catalyst was prepared by a simple hydrothermal treatment method. The results showed that there was an improvement in both the reaction rate and the mineralization degree when  $\text{TiO}_2$  was modified with graphene. This higher efficiency could be attributed to the increase of the active sites for adsorption of BPA, to the more effective use of solar spectrum, to the inhibition of electron-hole recombination and the increase of catalyst efficiency by the charge migration between  $\text{TiO}_2$  and graphene. Experimental results showed that 20 and 120 min of  $25\text{--}30\text{ W m}^{-2}$  solar irradiation were required to degrade  $2.5\text{ mg L}^{-1}$  Bisphenol-A and 84% solution TOC, respectively, when  $250\text{ mg L}^{-1}$   $\text{TiO}_2$ /graphene-2 wt% was used. Superoxide radical,  $\text{O}_2^{\bullet-}$ , was found to be the primary species contributing to the degradation of BPA in both solar/ $\text{TiO}_2$  and solar/ $\text{TiO}_2$ /graphene systems. In the case of solar/ $\text{TiO}_2$  reaction, hydroxyl radicals,  $\text{HO}^\bullet$ , played a less important role than that of singlet oxygen, due to the participation of  $\text{HO}^\bullet$  radicals instead of  $\text{h}^+$  in the reaction with  $\text{O}_2^{\bullet-}$  to form singlet oxygen. It can be concluded that this solar photocatalytic

517 TiO<sub>2</sub>/graphene oxidation system can be a potential alternative to degrade wastewater  
518 containing emerging contaminants, such as bisphenol-A.

519

## 520 **5. ACKNOWLEDGMENTS**

521 Financial support from MINECO (CTM2013-44317-R) is gratefully acknowledged.

522

## 6. REFERENCES

Akhavan, O., Ghaderi, E., 2009. Photocatalytic Reduction of Graphene Oxide Nanosheets on TiO<sub>2</sub> Thin Film for Photoinactivation of Bacteria in Solar Light Irradiation. J. Phys. Chem. C 113, 20214–20220.

Bellobono, I. R., Morazzoni, F., Bianchi, R., Mangone, E.S., Stanescu, R., Costache, C., Tozzi, P.M., 2005. Solar energy driven photocatalytic membrane modules for water reuse in agricultural and food industries. Pre-industrial experience using s-triazines as model molecules. Int. J. Photoenergy 7, 87-94.

Bielski, B.H.J., Cabelli, D.E., Arudi, R.L., Ross, A.B., 1985. Reactivity of HO<sub>2</sub><sup>•</sup>/O<sub>2</sub><sup>•-</sup> Radicals in Aqueous Solution. J. Phys. Chem. Ref. Data 14, 1041-1100.

Crain, D.A. Eriksen, M., Iguchi, T., Jobling, S., Laufer, H., LeBlanc, G.A., Guillete, Jr. L.J., 2007. An ecological assesment of Bisphenol-A: Evidence from comparative biology. Reprod. Toxicol. 24, 225-239.

Daimon, T., Hirakawa, T., Kitazawa, M., Suetake, J., Nosaka, Y., 2008. Formation of singlet molecular oxygen associated with the formation of superoxide radicals in aqueous suspensions of TiO<sub>2</sub> photocatalysts. Appl. Catal. A: Gen. 340, 169-175.



544 Daneshvar, N., Rabbani, M., Modirshahla, N., Behnajady, M.A., 2004. Kinetic  
 545 modelling of photocatalytic degradation of Acid Red 27 in UV/TiO<sub>2</sub> process. J.  
 546 Photoch. Photobio. A: 168, 39-45.

547

548 Durán, A., Monteagudo, J.M., San Martín, I., Sánchez-Romero, R., 2009. Photocatalytic  
 549 treatment of IGCC power station effluents in a UV-pilot plant. J. Hazard. Mater., 167,  
 550 885-891.

551

552 Esplugas, S., Bila, D.M., Krause, L.G.T., Dezotti, M., 2007. Ozonation and advanced  
 553 oxidation technologies to remove endocrine disrupting chemicals (EDCs) and  
 554 pharmaceuticals and personal care products (PPCPs) in water effluents. J. Hazard.  
 555 Mater., 149, 631-642.

556

557 Fujishima, A., Zhang, X., Tryk, D.A., 2008. TiO<sub>2</sub> photocatalysis and related surface  
 558 phenomena. Surf. Sci. Rep. 63, 515-582.

559

560 Fukahori, S., Ichiura, H., Kitaoka, T., Tanaka, H., 2003. Capturing of bisphenol A  
 561 photodecomposition intermediates by composite TiO<sub>2</sub> zeolite sheets. Appl. Catal.  
 562 B:Environ. 46, 453-462.

563

564 Gultekin, I., Mavrov, V., Ince, N.H., 2009. Degradation of Bisphenol-A by ozonation. J.  
 565 Adv. Oxid. Technol. 12, 242-248.

566

567 Hassan, F.M., Chabot, V., Li, J., Kim, B.K., Ricardez-Sandoval, L., Yu, A., 2013.  
 568 Pyrrolic structure enriched nitrogen doped graphene for highly efficient next generation  
 569 supercapacitors. *J. Mater. Chem. A* 1, 2904-2912.  
 570  
 571 Ho Y.S., McKay, G., 1999. Pseudo-Second Order Model for Sorption Processes.  
 572 *Process. Biochem.* 34, 451-465.  
 573  
 574 Hu, J.Y., Chen, X., Tao, G., Kekred, K., 2007. Fate of endocrine disrupting compounds  
 575 in membrane bioreactor systems. *Environ. Sci. Technol.* 41, 4097-4102.  
 576  
 577 Hummers, W.S., Offeman, R.E., 1958. Preparation of graphite oxide. *J. Am. Chem. Soc.*  
 578 80, 1339-1339.  
 579  
 580 Jin, Z., Wang, X., Sun, Y., Ai, Y., Wang, X., 2015. Adsorption of 4-n-Nonylphenol and  
 581 Bisphenol-A on Magnetic Reduced Graphene Oxides: A Combined Experimental and  
 582 Theoretical Studies. *Environ. Sci. Technol.* 49, 9168–9175.  
 583  
 584 Konstantinou, I.K., Albanis, T.A., 2003. TiO<sub>2</sub>-assisted photocatalytic degradation of  
 585 azo dyes in aqueous solution: kinetic and mechanistic investigations. A review. *Appl.*  
 586 *Catal. B: Env.* 49, 1-14.  
 587  
 588 Kumordzi, G., Malekshoar, G., Yanful, E. K., Ray, A. K., 2016. Solar photocatalytic  
 589 degradation of Zn<sup>2+</sup> using graphene based TiO<sub>2</sub>. *Sep. Purif. Technol.* 168, 294-301.

590

591 Lagergren, S., 1898. Zur theorie der sogenannten adsorption gelöster stoffe. Kungliga  
592 Svenska Vetenskapsakademiens, Handlingar 24, 1-39.

593

594 Lellala, K., Namratha, K. Byrappa, K., 2016. Ultrasonication assisted mild solvothermal  
595 synthesis and morphology study of few-layered graphene by colloidal suspensions of  
596 pristine graphene. Oxide Microp. Mesop. Mater. 226, 522-529.

597

598 Li, W., Zhao, S., Qi, B., Du, Y., Wang, X., Huo, M., 2009. Fast catalytic degradation of  
599 organic dye with air and MoO<sub>3</sub>:Ce nanofibers under room condition. Appl. Catal. B:  
600 Environ. 92, 333-340.

601

602 Liao, G., Zhu, D., Zheng, J., Yin, J., Lan, B., Li, L., 2016. Efficient mineralization of  
603 bisphenol A by photocatalytic ozonation with TiO<sub>2</sub> –graphene hybrid. J. Taiwan Inst.  
604 Chem. E. 67, 300-305.

605

606 Luo, A., Yang, Y., Zhang, A., Wang, M., Li, Y., Bian, L., Jiang, F.,  
607 Pan, X., 2015. Hydrothermal synthesis of fluorinated anatase TiO<sub>2</sub>/reduced  
608 graphene oxide nanocomposites and their photocatalytic degradation of bisphenol A.  
609 Appl. Surf. Sci. 353, 469-479.

610

611 Malekshoar, G., Pal, K., He, Q., Yu, A., Ray, A. K., 2014. Enhanced Solar  
612 photocatalytic degradation of phenol with coupled graphene-based titanium dioxide and  
613 zinc oxide. Ind. Eng. Chem. Res. 53, 18824-18832.

614

615 Monteagudo, J.M., Durán, A., San Martín, I., Carnicer, A., 2011. Roles of different  
616 intermediate active species in the mineralization reactions of phenolic pollutants under a  
617 UV-A/C photo-Fenton process. *Appl. Catal. B: Environ.* 106, 242-249.

618

619 Muruganandham, M., Swaminathan, M., 2004. Solar photocatalytic degradation of a  
620 reactive azo dye in TiO<sub>2</sub>-suspension. *Sol. Energy Mater. Sol. Cells* 81, 439-457.

621

622 Ni, M., Leung, M.K.H., Leung, D.Y.C., Sumathy, K., 2007. A review and recent  
623 developments in photocatalytic water-splitting using for hydrogen production. *Renew.*  
624 *Sustain. Energy Rev.* 11, 401-425.

625

626 Patterson, A.L., 1939. The Scherrer Formula for X-Ray Particle Size Determination.  
627 *Phys. Rev.* 56, 978- 982.

628

629 Pérez, M., Torrades, F., Domenech, X., Peral, J., 2002. Fenton and photo-Fenton  
630 oxidation of textile effluents. *Wat. Res.* 36, 2703-2710.

631

632 Robert, D., Piscopo, A., Weber, J.V., 2004. Selective solar photodegradation of  
633 organopollutant mixtures in water. *Sol. Energy* 77, 553-558.

634

635 Rogers, J.A., Metz, L., Yong, V.W., 2013. Review: Endocrine disrupting chemicals and  
 636 immune responses: A focus on Bisphenol-A and its potential mechanisms. *Mol.*  
 637 *Immunol.* 53, 421-430.

638

639 Rubin, B.S., 2011. Bisphenol-A: An endocrine disruptor with widespread exposure and  
 640 multiple effects. *J. Steroid. Biochem. Mol. Biol.* 127, 27-34.

641

642 Saha, S., Wang, J.M., Pal, A., 2012. Nano silver impregnation on commercial TiO<sub>2</sub> and  
 643 a comparative photocatalytic account to degrade malachite Green. *Sep. Purif. Technol.*  
 644 89, 147-159.

645

646 Sanchez-Polo, M., Abdel daïem, M.M., Ocampo-Perez, R., Rivera-Utrilla, J., Mota,  
 647 A.J., 2013. Comparative study of the photodegradation of Bisphenol A by HO<sup>•</sup>, SO<sub>4</sub><sup>•-</sup>  
 648 and CO<sub>3</sub><sup>-</sup>/HCO<sub>3</sub><sup>-</sup> radicals in aqueous phase. *Sci. Total Environ.* 463–464, 423–431.

649

650 Saran M., Summer, K.H., 1999. Assaying for hydroxyl radicals: hydroxylated  
 651 terephthalate is a superior fluorescence marker than hydroxylated benzoate. *Free Rad*  
 652 *Res.* 31, 429-436.

653

654 Schafer, T.E., Lapp, C.A., Hanes, C.M., Lewis, J.B., Wataha, J.C., Schuster, G.S., 1999.  
 655 Estrogenicity of bisphenol A and bisphenol A dimethacrylate in vitro. *J. Biomed. Mater.*  
 656 *Res.* 45, 192-197.

657

658 Shen, Y., Fang, Q.L., Chen, B.L., 2014. Environmental applications of three-  
 659 dimensional graphene-based macrostructures: adsorption, transformation, and detection.  
 660 Environ. Sci. Technol. 49, 67–84.  
 661

662 Upadhyay, R.K., Soin, N., Roy, S.S., 2014. Role of graphene/metal oxide composites as  
 663 photocatalysts, adsorbents and disinfectants in water treatment: a review. RSC Adv. 4,  
 664 3823-3851.  
 665

666 Wang, R.C., Yu, C.W., 2013. Phenol degradation under visible light irradiation in the  
 667 continuous system of photocatalysis and sonolysis. Ultrason. Sonochem. 20, 553–564.  
 668

669 Xekoukoulotakis, N.P., Drosou, C., Brebou, C., Chatzisyneon, E., Hapeshi, E., Fatta-  
 670 Kassinos, D., Mantzavinos, D., 2011. Kinetics of UV-A/TiO<sub>2</sub> photocatalytic  
 671 degradation and mineralization of the antibiotic sulfamethoxazole in aqueous matrices.  
 672 Catal. Today, 161, 163-168.  
 673

674 Yanga, L., Lia, Z., Jianga, H., Jianga, W., Sua, R., Luoa, S., Luoa, Y., 2016.  
 675 Photoelectrocatalytic oxidation of bisphenol A over mesh of TiO<sub>2</sub>/graphene/Cu<sub>2</sub>O.  
 676 Appl. Catal. B:Environ. 183, 75-85.  
 677

678 Yoon, S.H., Jeong, S., Lee, S., 2012. Oxidation of Bisphenol A by UV/S<sub>2</sub>O<sub>8</sub><sup>2-</sup>: a  
 679 comparison with UV/H<sub>2</sub>O<sub>2</sub>. J. Environ. Technol. 33, 123–128.  
 680

681 Young, T., Geng, M., Thagard, C.A., 2013. Oxidative degradation of Bisphenol A: a  
682 comparison between Fenton reagent, UV, UV/H<sub>2</sub>O<sub>2</sub> and Ultrasound. J. Adv. Oxid.  
683 Technol. 16, 89–101.

684

685

686

**Figure captions:**

**Figure 1:** a) Structure and properties of Bisphenol-A; b) Schematic illustration of the experimental set-up.

**Figure 2:** Normalized UV–vis diffuse reflectance spectra (DRS) of  $\text{TiO}_2$  and  $\text{TiO}_2/\text{graphene}$ -2 wt% composite.

**Figure 3:** a) XRD pattern of  $\text{TiO}_2$ ; b) XRD pattern of  $\text{TiO}_2/\text{graphene}$ ; c,d) TEM images of  $\text{TiO}_2/\text{graphene}$  nanocomposite; e) TEM images of graphene sheets; f) TEM images of  $\text{TiO}_2$  spheres.

**Figure 4:** a) Pseudo-first-order kinetics for the adsorption of BPA on  $\text{TiO}_2$  surface; b) Pseudo-first-order kinetics for the adsorption of BPA on  $\text{TiO}_2/\text{graphene}$  surface; c) Pseudo-second-order kinetics for the adsorption of BPA on  $\text{TiO}_2$  surface; d) Pseudo-second-order kinetics for the adsorption of BPA on  $\text{TiO}_2/\text{graphene}$  surface.

**Figure 5:** a) Mineralization degree of BPA solutions under the  $\text{TiO}_2/\text{graphene}$  photocatalyst with 1, 2 and 3 wt% of graphene. b) Effect of weight percentage of graphene in the  $\text{TiO}_2/\text{graphene}$  composite on the pseudo-first-order kinetic rate constant. Experimental conditions:  $[\text{BPA}]$ :  $2.5 \text{ mg L}^{-1}$ ;  $[\text{TiO}_2]$ :  $250 \text{ mg L}^{-1}$ ; solar power: 25-30  $\text{W/m}^2$ ; average temperature:  $26^\circ\text{C}$ ; reaction time: 120 min.

**Figure 6:** Evolution of the concentration of hydroxyl radicals and dissolved oxygen along the BPA degradation reaction. a-b) solar/ $\text{TiO}_2$  process: Influence of the initial BPA concentration,  $[\text{TiO}_2]$ :  $125 \text{ mg L}^{-1}$ ; c-d) solar/ $\text{TiO}_2$  and solar/ $\text{TiO}_2/\text{graphene}$



processes: Effect of TiO<sub>2</sub> loading, [BPA]: 5 mg L<sup>-1</sup>. Solar power: 25-30 W/m<sup>2</sup>; average temperature: 26°C; reaction time: 120 min.

**Figure 7:** Roles played by different intermediate oxidative species in the degradation of BPA solutions under a) solar TiO<sub>2</sub> process; b) solar TiO<sub>2</sub>/graphene process. Experimental conditions: [BPA]: 2.5 mg L<sup>-1</sup>; [TiO<sub>2</sub>/graphene]: 250 mg L<sup>-1</sup>/2 %wt; solar power: 25-30 W/m<sup>2</sup>; average temperature: 26°C; reaction time: 120 min.

**Table 1. N<sub>2</sub> adsorption-desorption characteristics of pure TiO<sub>2</sub> P25 and TiO<sub>2</sub>/graphene-2 wt% composites**

Sample	Surface area <sup>a</sup> (m <sup>2</sup> g <sup>-1</sup> )	Pore volumen <sup>b</sup> (cm <sup>3</sup> g <sup>-1</sup> )	Average pore size <sup>c</sup> (nm)
TiO <sub>2</sub> P25	50.56	0.27	19.99
TiO <sub>2</sub> /graphene	55.41	0.46	28.84

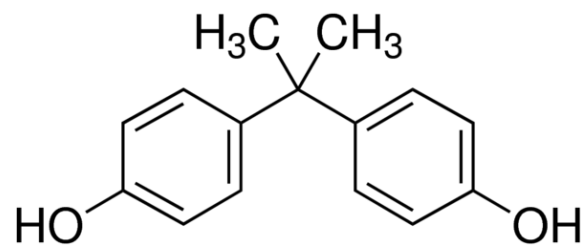
<sup>a</sup> BET specific surface area was calculated from the linear part of the corresponding BET plot.

<sup>b</sup> BJH desorption cumulative pore volume between 1.7 and 300 nm diameters.

<sup>c</sup> Average pore diameter was estimated from the BJH formula

**Table 2. Kinetic parameters for the adsorption of BPA by TiO<sub>2</sub> or by TiO<sub>2</sub>/graphene**

Pseudo-second-order				
TiO <sub>2</sub>			TiO <sub>2</sub> /graphene	
	pH 2.5	pH 7.5	pH 2.5	pH 7.5
<i>Q<sub>e</sub></i> (mg/g)	18.149	18.248	31.056	31.056
<i>k<sub>2</sub></i> (g min <sup>-1</sup> mg <sup>-1</sup> )	0.0007	0.0037	0.0029	0.0043

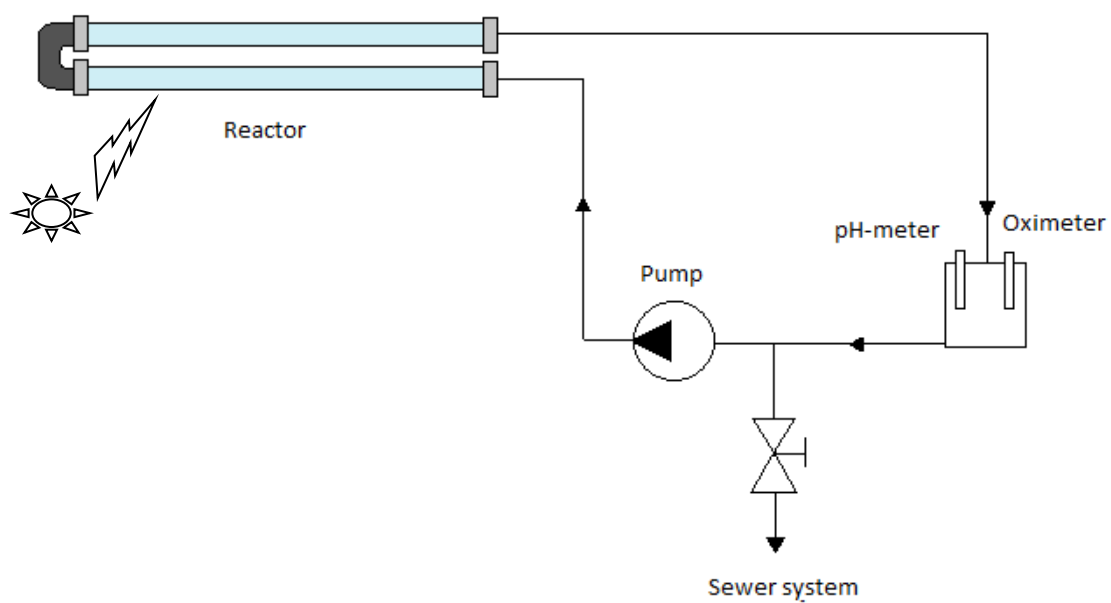


Linear formula:  $(\text{CH}_3)_2\text{C}(\text{C}_6\text{H}_4\text{OH})_2$

Molecular weight:  $228.29 \text{ g mol}^{-1}$

Water solubility:  $120 \text{ mg L}^{-1}$  ( $25^\circ\text{C}$ )

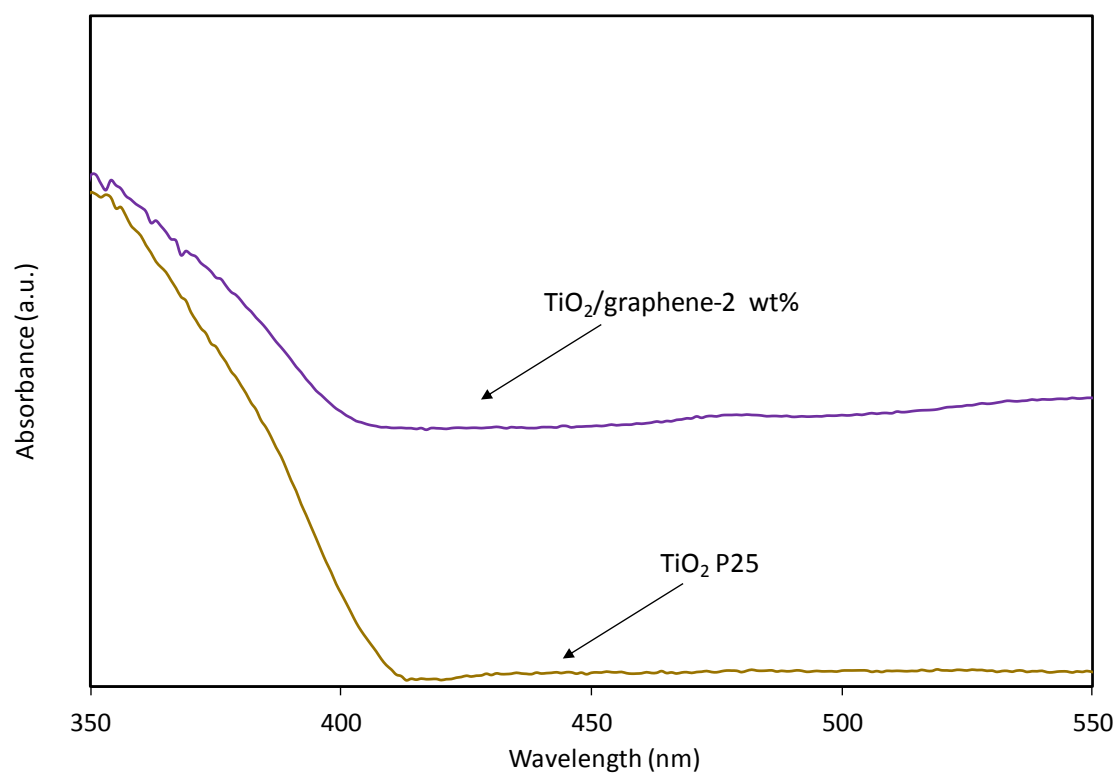
a)



b)

**Figure 1**

756



757

758

759 **Figure 2**

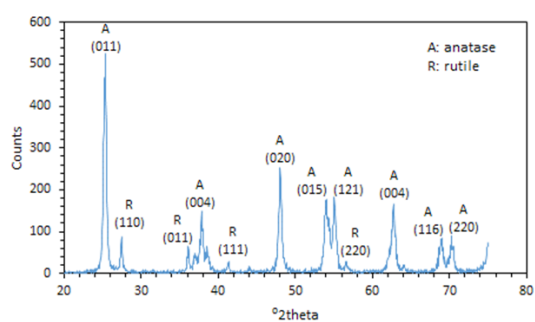
760

761

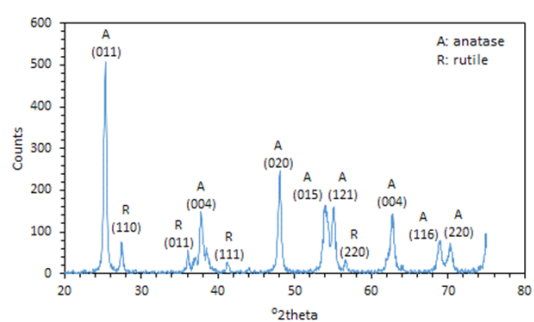
762

763

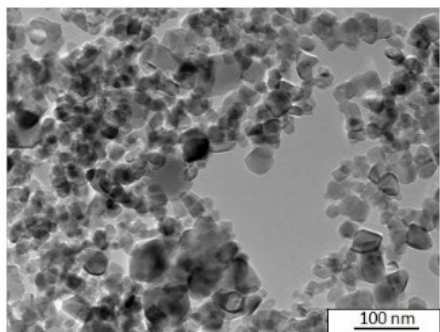
764



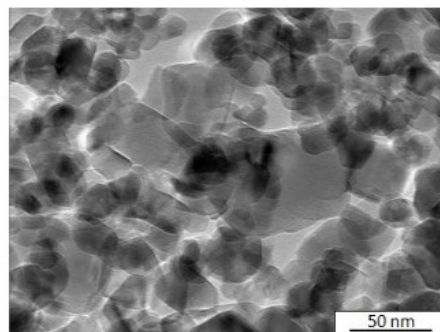
a)



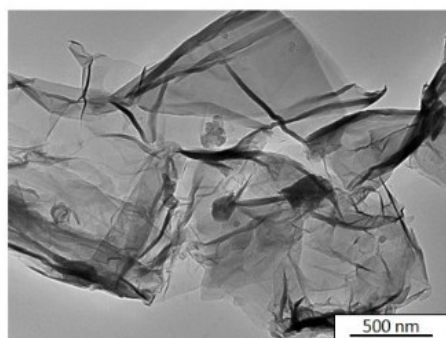
b)



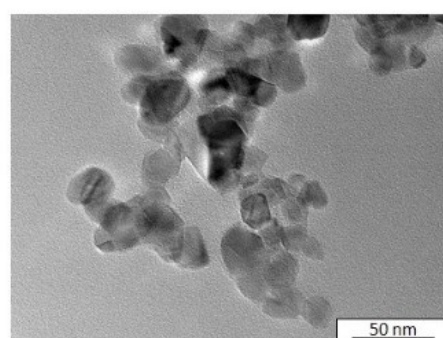
c)



d)



e)



f)

765

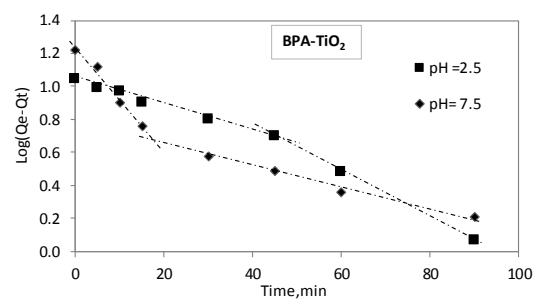
766 **Figure 3**

767

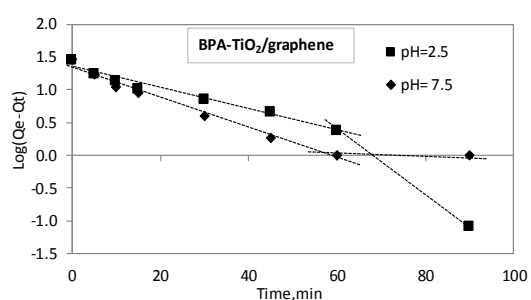
768

769

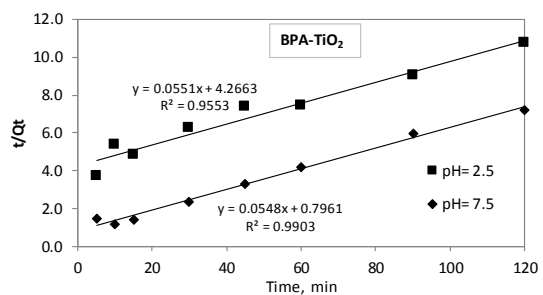
770



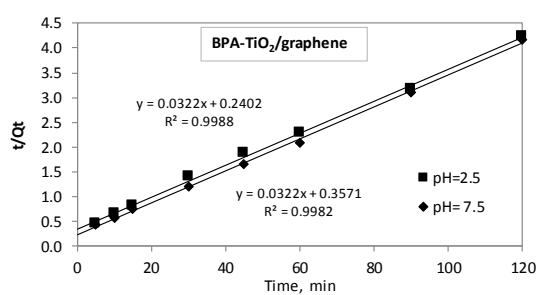
a)



b)

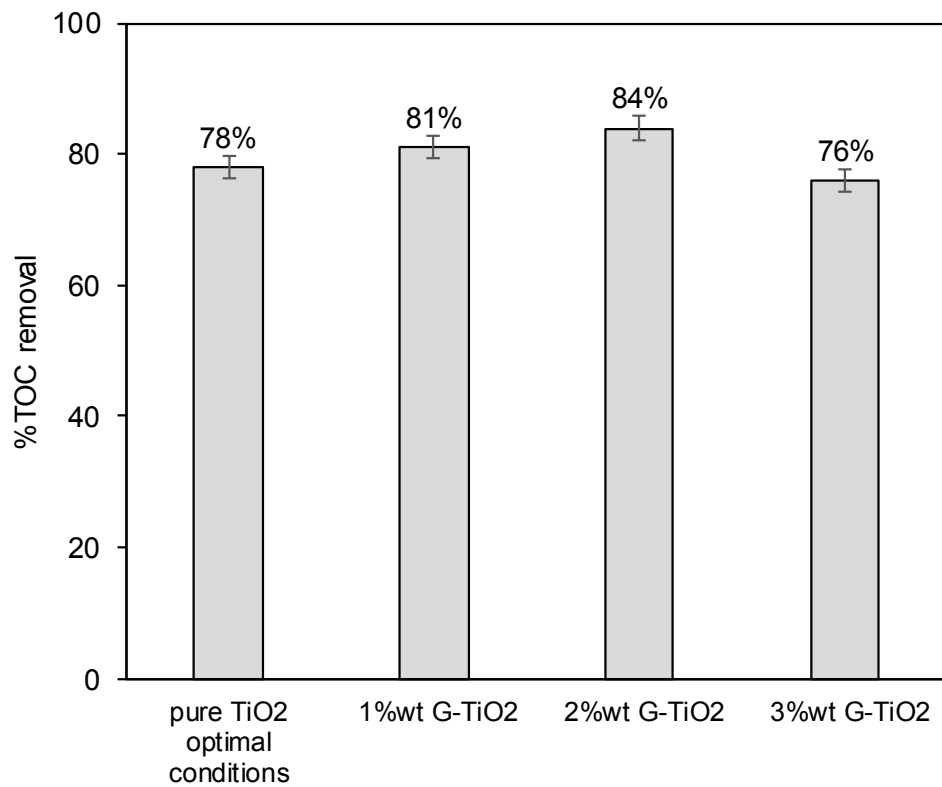


c)

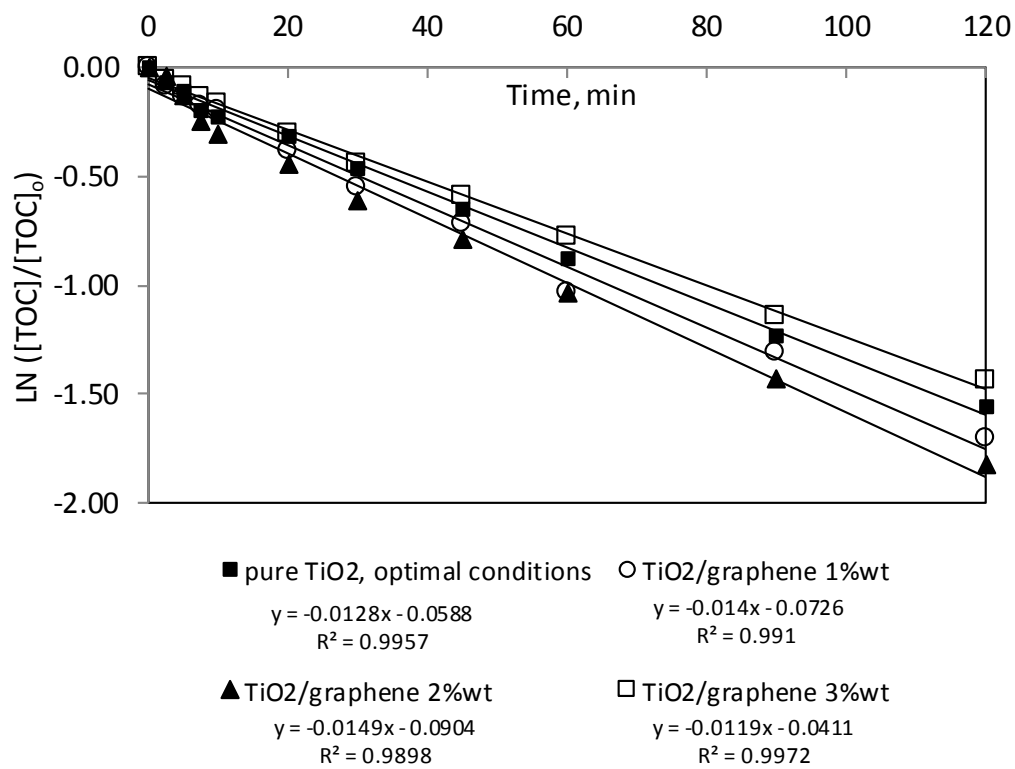


d)

**Figure 4**

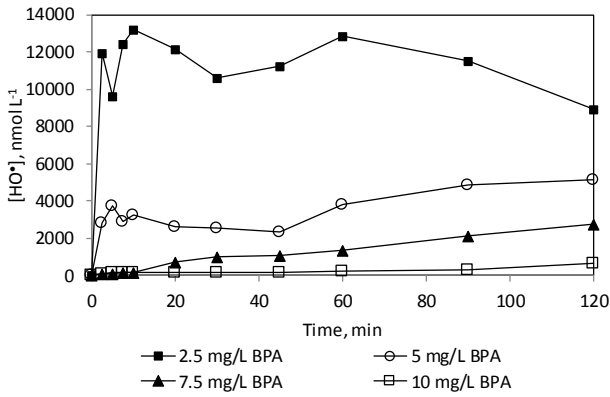


a)

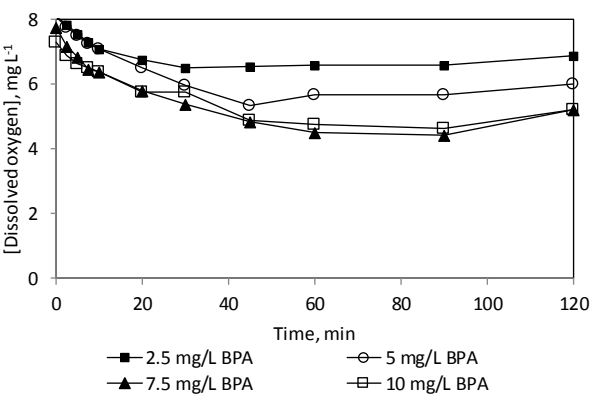


b)

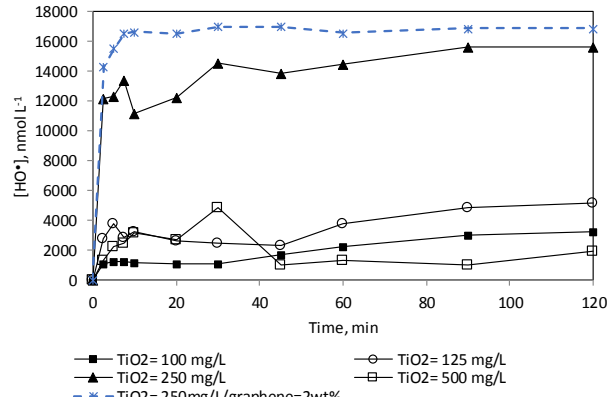
**Figure 5**



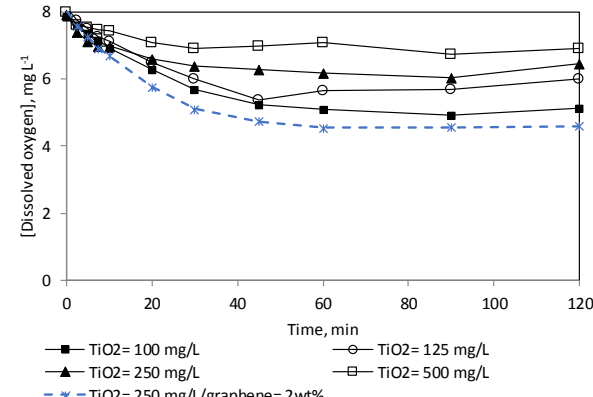
a)



b)



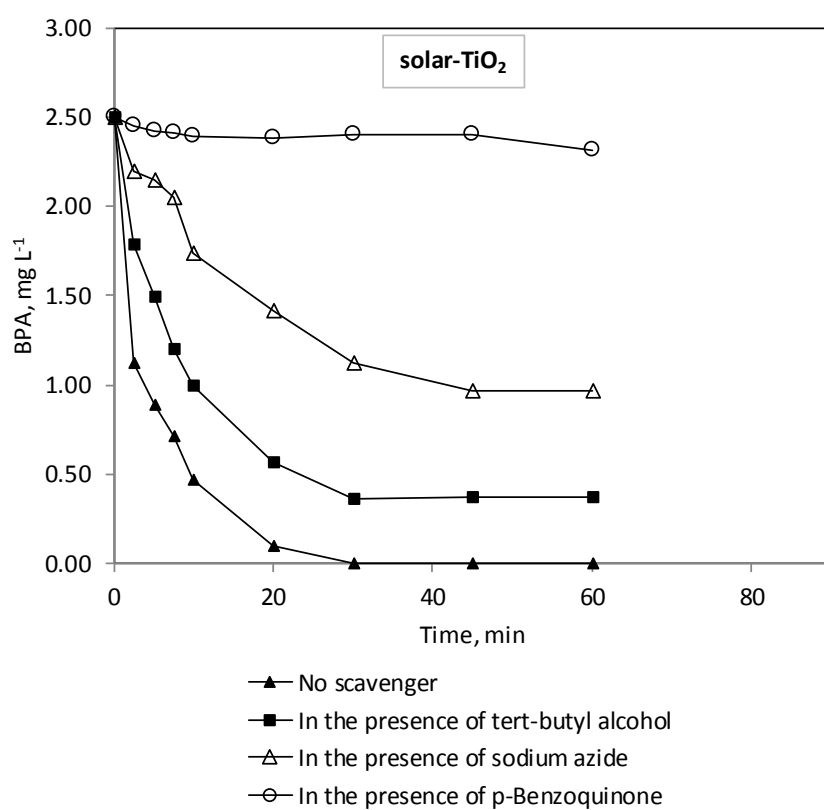
c)



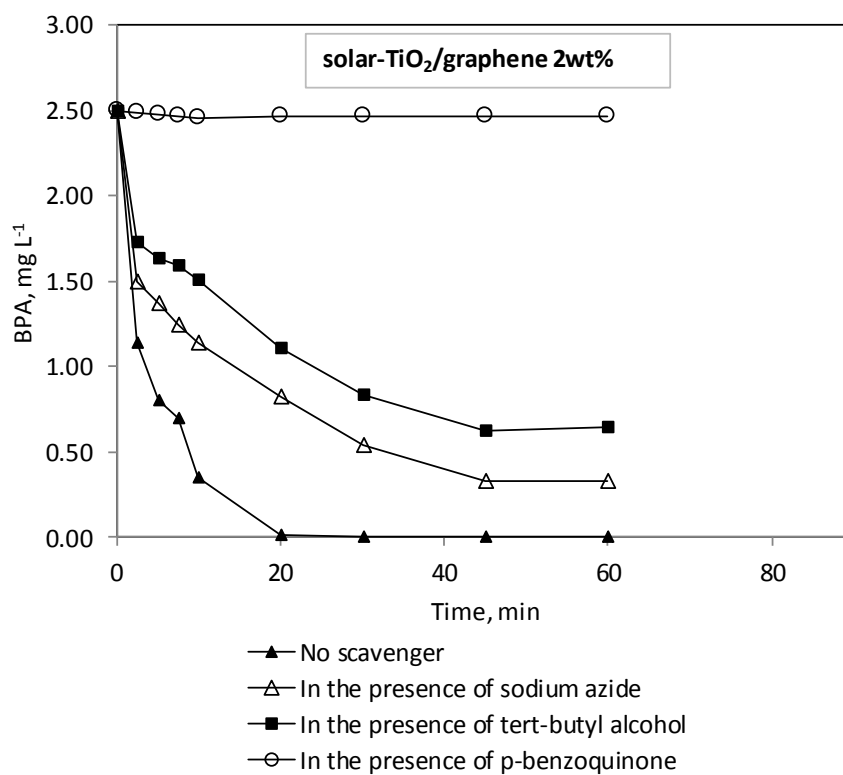
d)

**Figure 6**





a)



b)

782 **Figure 7**